Landscape and Urban Planning 163 (2017) 107–120

Contents lists available at ScienceDirect

Landscape and Urban Planning

journal homepage: www.elsevier.com/locate/landurbplan

Research Paper

On the association between land system architecture and land surface temperatures: Evidence from a Desert Metropolis—Phoenix, Arizona, U.S.A

Xiaoxiao Li [a,*], Yiannis Kamarianakis [b], Yun Ouyang [c], Billie L. Turner II [d], Anthony Brazel [e]

[a] School of Geographical Sciences & Urban Planning, Julie Ann Wrigley Global Institute of Sustainability, Central Arizona-Phoenix Long-Term Ecological Research, Arizona State University, Tempe, AZ 85287-5302, United States
[b] School of Mathematics & Statistical Sciences, College of Liberal Arts and Sciences, Arizona State University, Tempe, AZ 85287-1804, United States
[c] Enterprise Data and Analytics Office, USAA, 1 Norterra Drive, Phoenix, AZ 85085, United States
[d] School of Geographical Sciences & Urban Planning, School of Sustainability, Arizona State University, Tempe, AZ 85287-5302, United States
[e] School of Geographical Sciences & Urban Planning, Arizona State University, Tempe, AZ 85287-5302, United States

HIGHLIGHTS

- Land system architecture affects land surface temperature (LST) of residential parcels.
- Land-cover composition has the largest effect on LST but land-cover configuration is significant.
- Compact and concentrated land-covers, foremost vegetation, improves nighttime cooling.
- Large land-cover units of irregular shape improve daytime cooling.
- Parcel level land architecture can be used to mitigate the LST of residences.

ARTICLE INFO

Article history:
Received 23 March 2016
Received in revised form 3 February 2017
Accepted 14 February 2017
Available online 31 March 2017

Keywords:
Land system architecture
Linear mixed-effects models
MODIS/ASTER
Urban heat island effect
Land surface temperature
NAIP
Parcel scale

ABSTRACT

The relationship between the characteristics of the urban land system and land surface temperature (LST) has received increasing attention in urban heat island and sustainability research, especially for desert cities. This research generally employs medium or coarser spatial resolution data and primarily focuses on the effects of a few classes of land-cover composition and pattern at the neighborhood or larger level using regression models. This study explores the effects of land system architecture—composition and configuration, both pattern and shape, of fine-grain land-cover classes—on LST of single family residential parcels in the Phoenix, Arizona (southwestern USA) metropolitan area. A 1 m resolution land-cover map is used to calculate land architecture metrics at the parcel level, and 6.8 m resolution MODIS/ASTER data are employed to retrieve LST. Linear mixed-effects models quantify the impacts of land configuration on LST at the parcel scale, controlling for the effects of land composition and neighborhood characteristics. Results indicate that parcel-level land-cover composition has the strongest association with daytime and nighttime LST, but the configuration of this cover, foremost compactness and concentration, also affects LST, with different associations between land architecture and LST at nighttime and daytime. Given information on land system architecture at the parcel level, additional information based on geographic and socioeconomic variables does not improve the generalization capability of the statistical models. The results point the way towards parcel-level land-cover design that helps to mitigate the urban heat island effect for warm desert cities, although tradeoffs with other sustainability indicators must be considered.

1. Introduction

Over a quarter century ago, Forman (1990) called for ecological research on landscape mosaics (land-cover composition and configuration) in regard to the environmental performance and sustainability of landscapes (also Wu, 2013), and more recently has championed this approach for urban ecology (Forman, 2014). Urban

* Corresponding author.
E-mail addresses: xiaoxia4@asu.edu (X. Li), yiannis76@asu.edu (Y. Kamarianakis), yun.ouyang.1@gmail.com (Y. Ouyang), Billie.L.Turner@asu.edu (B.L. Turner II), abrazel@asu.edu (A. Brazel).

http://dx.doi.org/10.1016/j.landurbplan.2017.02.009
0169-2046/

climatology, in turn, has long considered the impacts of urban morphology or geometry on the urban heat island (UHI) effect. Much attention has been given to the vertical dimensions and spacing of buildings (e.g., urban canyon height-to-width ratios), sky-views, and the density of general types of land covers, such as vegetation and impervious surfaces (e.g., Stewart & Oke, 2012). In addition, landscape architecture has long addressed the structure of outdoor spaces, foremost parks and common and reclamation areas, with a strong orientation towards their aesthetics attributes. It has drawn on ecological principles in landscape design, however, more so than examining the environmental dynamics of existing landscape conditions (Brown & Corry, 2011; Yu, Li, & Ji, 2001).

Joining these research interests and the approaches applied to them, but differing somewhat from each, is the transdisciplinary subfield of land system (change) science, focused on the causes and consequences of land change (Turner et al., 2007). Land system science, partly a product of global environmental change and sustainability interests, seeks to provide a science-based understanding of land-use and –cover change, increasingly with an eye towards informing decision making. Land system architecture (henceforth, land architecture) is one dimension of this effort (Janetos, Verbug, & Murray, 2013). It addresses the composition and configuration of land covers, including pattern, shape and connectivity, and their impacts on social-environmental system performance (Turner, 2017). It differs slightly from landscape mosaic approaches in its attention to fine-grain spatial analysis (i.e., 1–30 m), and detailed categories of land covers (e.g., among various categories of vegetation cover) and, in some cases, land uses. These distinctions make the land architecture orientation well fit to address the heterogeneous character of urban land cover, and compatible with calls for land system science to address urbanization-land relationships (e.g., Seto and Reenberg, 2014). Land architecture explores configuration metrics derived from the spatial sciences rather than relying solely on those developed in ecology (see below). Urban land architecture has focused on the UHI effect (Turner, 2017), but differs from urban morphology or geometry in regard to the array of land-cover categories examined and the details of configuration. Finally, the focus of land architecture (as defined here) on base research to inform decision making about sustainability problems (Clark, 2007) distinguishes it from the primary motivation of activities within the subfield of landscape architecture.

The UHI effect increasingly captures the attention of administrators and decision makers concerned with mitigating urban temperature extremes and their impacts on energy and water use, human health, and thermal comfort (e.g., City of Phoenix, 2010; Kleerekoper, van Esch, & Baldiri Salcedo, 2012; Shashua-Bar, Pearlmutter, & Erell, 2009, Shashua-Bar, Pearlmutter, & Erell, 2011; Solecki et al., 2005; Wentz, Rode, Li, & Tellman, 2016). This concern, in turn, has drawn insights from UHI research undertaken in the subfields and approaches discussed above as well as in remote sensing (e.g., Gago, Roldán, Pacheco-Torres, & Ordoñez, 2013; Hart & Sailor, 2009; Oke, 1981; Taha, 1997). The problem and the research given to it are particularly acute for urban areas worldwide situated in warm and hot climates where the UHI effect is expected to be significantly amplified by global climate warming (e.g., Grossman-Clarke, Schubert, Clarke, & Harlan, 2014; McCarthy, Best, & Betts, 2010; Saha, Davis, & Hondula, 2014).

With these concerns in mind, the role of urban land composition and configuration on the UHI and its capacity to mitigate the phenomenon has been examined in regard to both air and land surface temperature, including the role of "smart buildings", green and white roofs, urban street canyons, green spaces, shade, impervious surfaces, bare soil, and sky-views (e.g., Coseo & Larsen, 2014; Donovan & Butry, 2009; Erellet al., 2012; Giridharan, Lau, Ganesan, & Givoni, 2007; Li, Bou-Zeid, & Oppenheimer, 2014; Oke, 1981; Santamouris, 2013). Configuration has largely been addressed in terms of the spatial distribution or pattern of general types of land covers (Buyantuyev & Wu, 2010; Middel, Häb, Brazel, Martin, & Guhathakurta, 2014; Myint, 2012; Myint, Wentz, Brazel, & Qualttrochi, 2013; Stewart and Oke, 2012), with abundant attention to Chinese cities (e.g., Huang, Li, Zhao, & Zhu, 2008; Li, Wang, Wang, Ma, & Zhang, 2009; Su, Gu, & Yang, 2010; Zhang et al., 2013).

Complementing recent research that treats land configuration in rural, forest landscapes (Mitchell, Bennett, & Gonzalez, 2013; Wu, Jenerette, Buyantuyev, & Redman, 2011) and consistent with Forman's (1990) call, nascent efforts are underway to determine the role of land architecture, as defined here, on the UHI effect. Most studies to date tend to employ 30 m or coarser resolution satellite data to calculate daytime land surface temperature (LST) of urban land units, address one or two land-covers at the neighborhood or larger level, use FRAGSTATS metrics (McGarigal and Marks, 1995; McGarigal, Cushman, & Ene, 2012) to determine land-cover configuration, and apply regression models to assess the land cover-LST relationship (e.g., Turner, 2017). The results indicate that the concentration of different land covers in Phoenix and Las Vegas (USA) increased heating or cooling effects (Fan, Myint, & Zheng, 2015; Myint et al., 2015; Zheng, Myint, & Fan, 2014), whereas different elements of shape (e.g., edge density) have a strong effect on land-cover temperature in Beijing, China (Li, Zhou, Ouyang, Xu, & Zheng, 2012), Baltimore, USA (Zhou, Huang, & Cadenasso, 2011), and Phoenix (Connors, Galletti, & Chow, 2013). Indeed, at least one study in Phoenix found land-cover shape at the parcel level, as measured by the Normalized Moment of Inertia, trumped land-cover pattern in terms of effects on LST at the neighborhood level (Li, Li, Middel, Harlan, & Brazel, 2016).

In addition to the overall work on the UHI effect, land architecture approaches increasingly point to the significant role that both the pattern and shape of small-size land covers have on temperature extremes. Here we extend this line of research by exploring the role of land configuration on LST at the single-family residential (SFR) parcel level for the metropolitan area of Phoenix, Arizona, U.S.A., using 2010–2011 data (Fig. 1). Consistent with most other studies, FRAGSTATS serve as the metrics of composition and configuration. Following Li et al. (2016), multiple land covers and their mosaics are examined. These land covers are linked to 6.8 m MASTER data in order to match the fine-resolution, heterogeneous land cover of the residential parcels. New to this assessment, both daytime and nighttime LST are analyzed. In addition, the neighborhood effect (Cox, 1969; Johnston, Propper, Sarker, Jones, & Bolster, 2005) on individual parcels is investigated using linear mixed effect models (LMEs). LMEs allow us to identify significant predictors related to land configuration while accounting for nested, neighborhood-specific data structures and controlling for land composition, socioeconomic neighborhood characteristics and spatial correlation of neighboring parcels. Evaluation of LMEs emphasized their generalization capability based on their performance in predicting outcomes on neighborhoods not used to estimate model parameters. Taken together, this study constitutes a novel attempt to determine the role of residential land architecture on the UHI effect, specifically the surface urban heat island (SUHI). The results have the potential to inform how a redesign or reshaping of the land units could mitigate the extremes of the SUHI.

2. Study site, data, and methods

2.1. Study site

The Phoenix metropolitan area (Fig. 1) consists of 26 joined cities and towns that housed about 4.2 million people in 2010 and covered over 7600 km^2 of the northern Sonoran Desert of

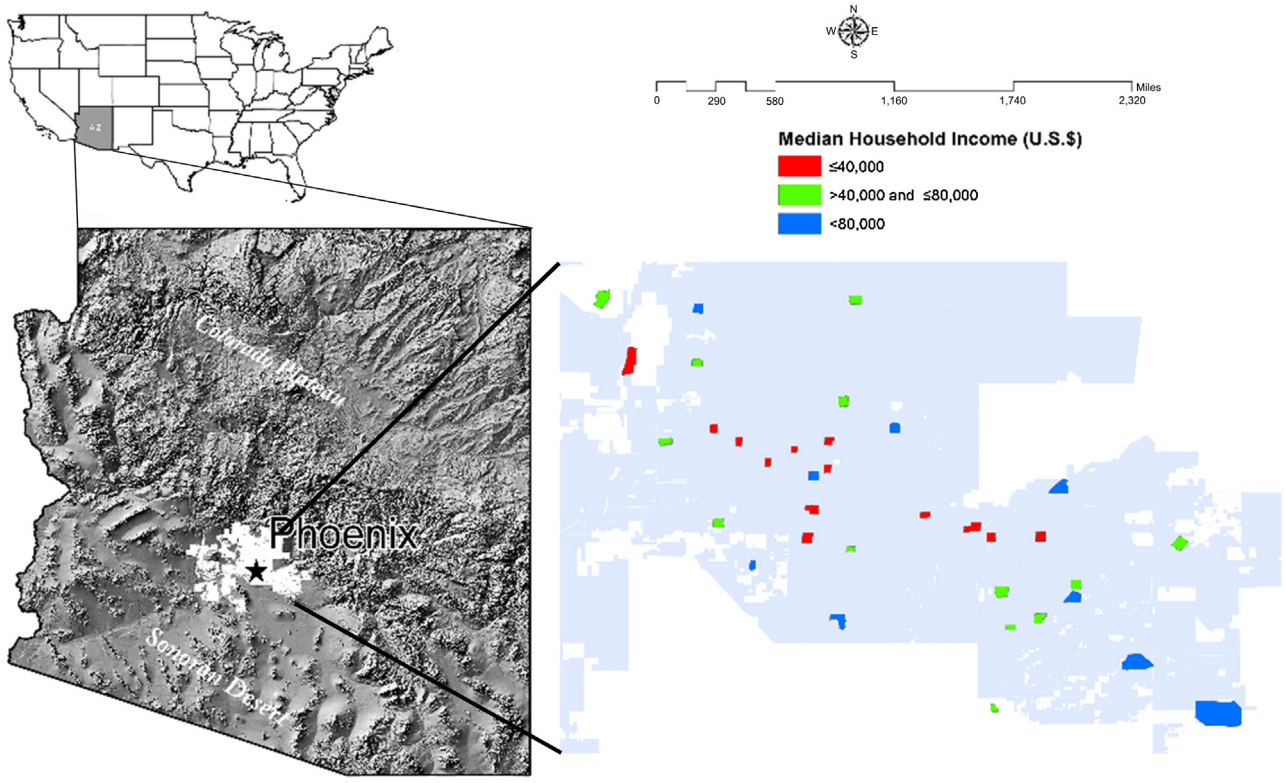

Fig. 1. Location of the Phoenix, Arizona, USA, metropolitan area in the American Southwest and the Household Income of the Sampled Neighborhoods.

Maricopa County, AZ. Rapid urbanization, largely at the expense of former irrigated farmlands (Keys, Wentz, & Redman, 2007; Grossman-Clarke, Zehnder, Loridan, & Grimmond, 2010) and the cooling effects that they render, has generated extreme heat problems, with maximum temperatures exacerbated by the SUHI effect (Buyantuyev & Wu, 2009; Chow, Chuang, & Gober, 2012). The average summer air temperature exceeds 30 °C, and the number of days in excess of 43 °C increased by 20 over the last decade (Connors et al., 2013; Jenerette, Harlan, Stefanov, & Martin, 2011). Interestingly, the SUHI effect relative to the ambient rural temperature is greater at night than day (Hawkins, Brazel, Stefanov, Bigler, & Saffell, 2004). Overall the SUHI in the greater Phoenix area raises a series of issues about water consumption—a highly constrained resource, the largest urban uses of which are irrigated, parcel-level vegetation and swimming pools—energy use, and public health (Harlan, Brazel, Prashad, Stefanov, & Larsen, 2006; Silva, Phelan, & Golden, 2010; Wentz et al., 2016). For these and other reasons, the City of Phoenix (2010) plans to respond to the UHI, in part, through greening its urban landscape.

2.2. Data collection and preparation

Three basic data sources are employed in this analysis (Fig. 2): (1) remotely sensed imagery (1 m), augmented by parcel information; (2) locational and socio-economic data; and (3) LST taken from remotely sensed imagery (6.8 m) matched to individual parcels.

2.2.1. Land-cover data

The data used to generate the land-cover classification and metrics (independent variables; see 2.3.1) for SFR parcels were generated from the 1 m resolution, 4-band orthophotography produced in 2010 by the National Agriculture Imagery Program (NAIP imagery). The classification utilized an object-based approach with expert knowledge decision rules, assisted by a cadastral vector layer as ancillary data (Li, Myint, Zhang, Galletti, & Zhang, 2014). Original NAIP imagery and cadastral shapefiles were pre-processed by two types of spectral transformation and one type of spatial enhancement. RGB to I transformation, Principal Components Analysis (PCA), Normalized Difference Vegetation Index (NDVI), and morphological convolution operations were employed. The output images from the transformation functions were merged with the original four-band images as the input data for an object-based image analysis.

The object-based method sets up a hierarchical network in which image objects at different levels are delineated according to their spectral, spatial, contextual, and geometrical characteristics correspondingly. A number of segmentation algorithms (multi-resolution, multi-threshold, Quadtree based, and chessboard segmentation) were executed for the hierarchical network, and at a finer image object level, the detailed land-cover classes were identified within parcels (Li, Myint, et al., 2014).

Twelve land-cover classes were distinguished, of which five are common to SFR parcels: building, bare soil/rock, tree/shrub, turf grass (henceforth, grass), and swimming pool. The impervious surfaces of driveways and sidewalks could not be consistently distinguished from bare soil/rock. Land covers adjacent to but not part of the SFRs, such as roads and playgrounds, were not considered in this analysis. We suspect minimal effects of these adjacent covers on parcel LST. Heat island research indicates a well-defined land-cover impact on LST when near-surface wind speeds are light, below 5 mph or 2.2 m s^{-1} (Fast, Torcolini, & Redman, 2005).

A total 12,265 SFRs in 35 neighborhoods were used to calculate the land architecture metrics for five land-cover types in each residential parcel. The parcels were delineated from the 2010 Maricopa County Tax Assessor roles, and ranged from 38 to 2643 per neighborhood. All SFR parcels do not contain a swimming pool and the variability of pool sizes is small. For this reason, the presence of

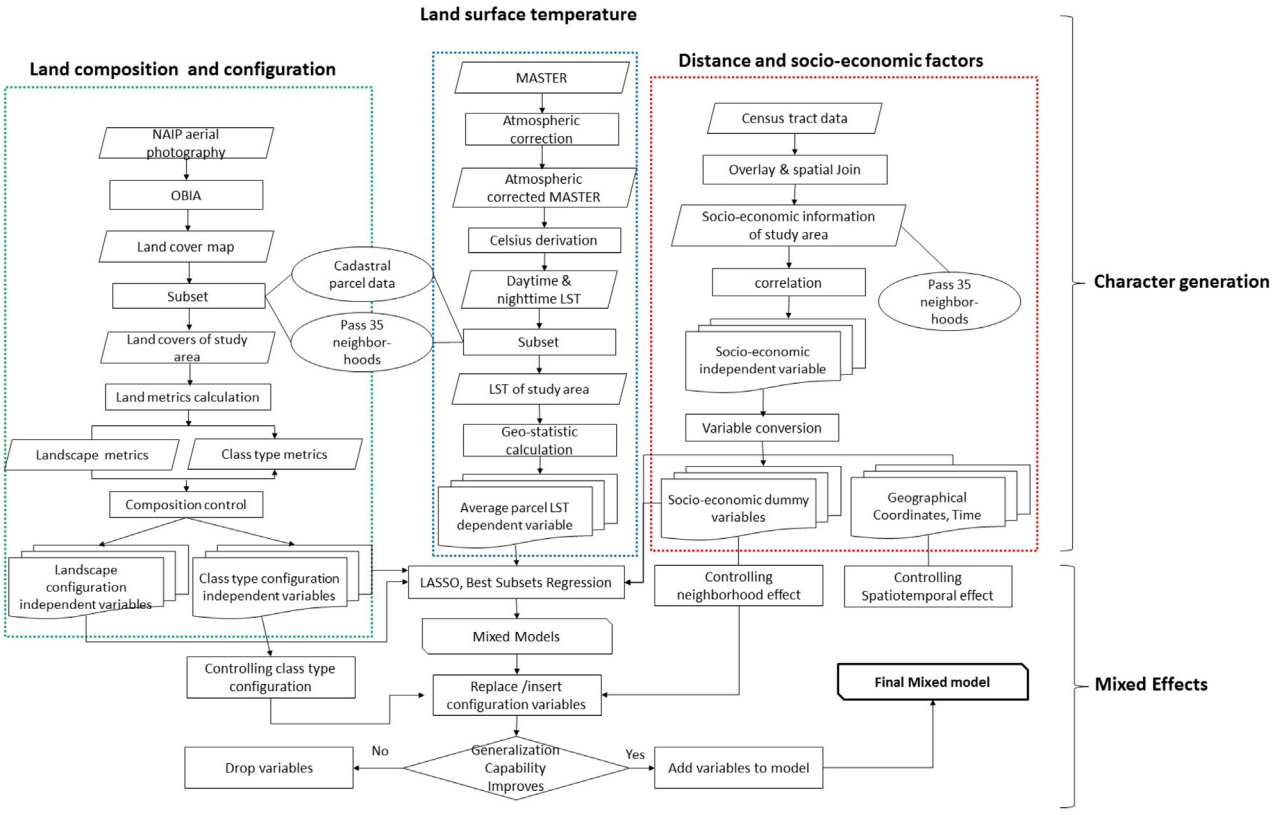

Fig. 2. Research design.

a pool was included as a factor variable in the statistical analysis. Examples of the land-cover results are provided in Fig. 3.

2.2.2. Land surface temperature data

The MODIS/ASTER Airborne Simulator (MASTER) was used to account for the fine-grain heterogeneous of the urban land covers. It is an imaging spectrometer that acquires high spectral and spatial resolution imagery with fifty channels ranging from 0.4–14 μm with an approximate 6.8 m pixel size (Hook, Myers, Thome, Fitzgerald, & Kahle, 2001; Chang, Han, Fan, Chen, & Chang, 2002). The MASTER data were acquired by flights during the daytime (11:55 a.m.–2:00 p.m., July 12, 2011; 11:15 a.m.–1:05 p.m., July 13, 2011) and nighttime (1:40 a.m.–4:10 a.m., July 15, 2011; 1:20 a.m.–3:10 a.m., July 16, 2011).

The MASTER data flight lines were segmented into smaller subsets in order to improve geo-referencing by minimizing distortions and removing erroneous data (for flight lines see: Jenerette et al., 2016). The LST was extracted and converted to °C using ENVI software and its atmospheric correction module: Quick Atmospheric Correction (Bernstein et al., 2005). The emissivity normalization function for thermal IR bands was applied on each of the subsets. The LST data were geo-referenced with NAIP orthophotography (Section 2.2.1) from Ground Control Points with ENVI software. These data were further extracted for each parcel polygon (obtained from cadastral GIS vector layer) to represent the parcel mean LST at daytime and nighttime. LSTs calculated this way are accurate for light wind conditions as noted above. For the dates in question the wind speeds for 52 weather stations across the metro-area were within the aforementioned limits. We assume, therefore, that near-surface winds did not affect our measures of LST, although each neighborhood examined did not have a weather station. Examples of the LST results are depicted in Fig. 3.

2.2.3. Socio-economic data

The Central Arizona-Phoenix Long-term Ecological Research project has identified 40 neighborhoods that capture the social-environmental diversity (e.g., income, ethnicity, landscaping preferences) within the metropolitan area. Socio-economic data from 35 neighborhoods were used as exploratory variables to address the possibility of neighborhood effects. In this case, the group or relational effects were the role of neighborhood parcels on an individual parcel. Socio-economic data for these neighborhoods were drawn from the 2010 U.S. Census and included median household income and age of residents and ethnicity. Each neighborhood was assigned to one of three locational categories: within the (1) central core or (2) not of their respective cities and (3) adjacent to the metropolitan fringe. Also, the ratio of living area divided by the total area of each parcel (P_LIVING; county assessor data) was calculated. This explanatory variable was included because preliminary analyses indicated that the percentage of the parcel area covered by buildings (P_BUILDING; see 2.3.1) was not strongly correlated with LST, a result that appeared to be counterintuitive.

2.3. Methods

2.3.1. Land architecture metrics

FRAGSTATS (or landscape metrics; Table 1) were developed for ecosystem and landscape research but have been employed in various research dealing with land configuration (McGarigal et al., 2012). To maintain consistency with this research, FRAGSTATS were used as independent, or predictor variables in our statistical models. Both disaggregate (land-cover specific) and aggregate (parcel level) metrics were used in the development of predictive models for LST. In order to maximally reduce the redundancy among the many FRAGSTATS metrics as well as to include as many important measurements as possible, five metrics (PLAND, PD, ED,

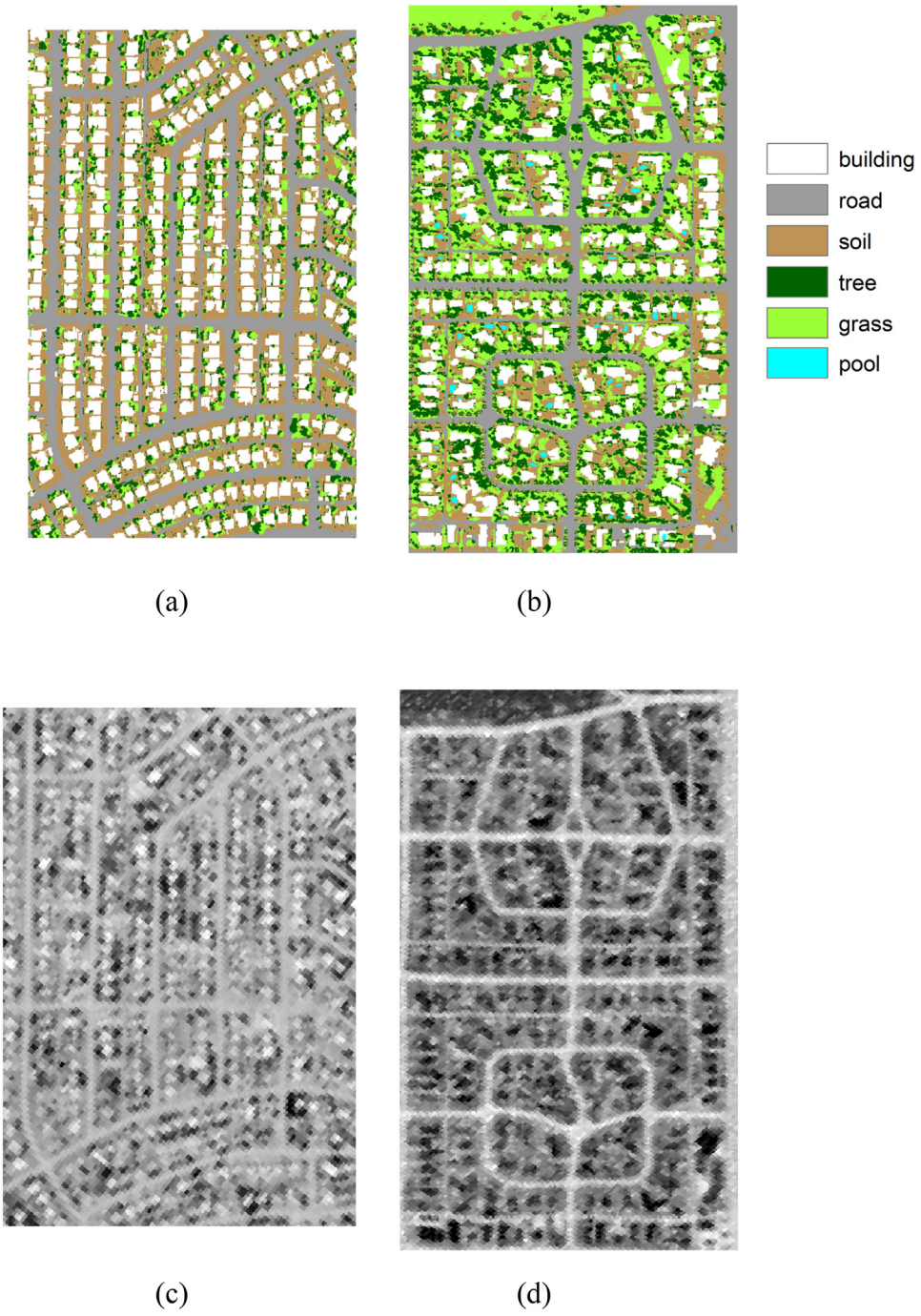

Fig. 3. Examples of the land cover of neighborhoods (1 m) and their land surface temperatures (LST) (6.8 m). (a) Low-level (xeric) and (b) high level (mesic) vegetated neighborhoods; (c) daytime LST of xeric and (d) nighttime LST of mesic neighborhoods.

LSI, FRAC) were chosen to quantify the character of each land-cover type. These five metrics were grouped in two categories: land composition (PLAND) and spatial configuration (the other four). PLAND measures the fraction of patches of each land-cover type within a unit, while the spatial configuration metrics characterize the shape complexity and spatial distribution of patches in the unit (Table 1). PLAND and six configuration metrics (PD, ED, LSI, FRAC, CONTAG, and SHDI) were selected to measure the aggregated architecture of land patches per parcel.

The metrics were calculated using the FRAGSTATS 4.2 software package, and obeyed the "8-cell rule" (consider all 8 adjacent cells, including the 4 orthogonal and 4 diagonal neighbors) in defining patch neighborhoods (McGarigal et al., 2012). Rather than using a fixed pixel size as the sample unit common to other studies (e.g., Connors et al., 2013), SFR parcels ranging from 372 m^2 to 6039 m^2 were addressed, permitting a more precise spatial fit among parcels, neighborhoods, and LST.

2.3.2. Statistical analysis

Linear mixed-effects models were employed to quantify the land architecture-LST relationship for summer nighttime and daytime, while accounting for the effects of time, land composition, socio-economic and locational predictors. LMEs can be viewed as generalizations of neighborhood-specific regression models,

Table 1
Land architecture metrics.

Metric/Abbreviation	Description	Class Specific Metrics	Aggregated Parcel Metrics
Percent cover of a land-cover class/PLAND	Proportion of the land-cover type (patch type) on the unit landscape plot ($0 < PLAND \leq 100$)	PLAND of Building, Soil, Soil, Tree/Shrub, Grass	N/A
Patch density/PD	Number of patches/ha (>0, determined by grain or pixel size)	PD of Building, Soil, Soil, Tree/Shrub, Grass	PD
Edge Density/ED	Total length of edges for all patches/ha ($\geq$0, where 0 refers to a landscape composed of one patch)	ED of Building, Soil, Soil, Tree/Shrub, Grass	ED
Landscape Shape index/LSI	Total length of all patch edges divided by the minimum possible length of the area of the unit landscape plot ($\geq$1, where the greater the LSI above 1 the more the shape deviates from a compact shape, i.e., a square)	LSI of Building, Soil, Soil, Tree/Shrub, Grass	LSI
Fractal dimension/ FRAC	A measure of shape complexity by calculating the departure of the patch from its Euclidean geometry ($1 \leq FRAC \leq 2$, where 1 corresponds to very simple shapes and 2 to extremely complex shapes)	FRAC of Building, Soil, Soil, Tree/Shrub, Grass	FRAC
Contagion/CONTAG	A measure of adjacency of patches ($0 < CONTAG \leq 100$, where patches are maximally disaggregated and dispersed when the values are small; 100 is the reverse)	N/A	CONTAG
Shannon's diversity index/SHDI	A measure of the diversity of patches (0 is a landscape with 1 patch)	N/A	SHDI

which summarize statistical associations when measurements are collected from a group of neighborhoods. In contrast with regression, the adopted model class provides valid inferences with regard to the significance of the predictors by accounting for nested, neighborhood-specific data structures and spatial correlation effects within each neighborhood. Parcels are sampled in clusters. Those from the same neighborhood are expected to be correlated. Ignoring the clustered data structure may lead to inappropriate estimates of standard errors of model parameters and consequently to errors in statistical inference due to inaccurate p-values. In addition to the underestimation of standard errors, by ignoring the multilevel structure of the data, important relationships involving each level of the data (e.g., important predictors that characterize neighborhoods; Finch, Bolin, & Kelley, 2014) may be missed.

The estimated models are formulated as:

$$\left.\begin{array}{c} \boldsymbol{Y}_i = \boldsymbol{X}_i \times \beta + \boldsymbol{Z}_i \times \boldsymbol{b}_i + \boldsymbol{\varepsilon}_i \\ \boldsymbol{b}_i \sim N(0, D) \\ \boldsymbol{\varepsilon}_i \sim N(0, \boldsymbol{\Sigma}_i) \\ \boldsymbol{b}_1, \ldots, \boldsymbol{b}_N, \boldsymbol{\varepsilon}_1, \ldots, \boldsymbol{\varepsilon}_N \ \textit{independent} \end{array}\right\}. \quad (1)$$

In (1), Y_i denotes the vector of observed LST in neighborhood i with $i = 1, \ldots, N$; its length depends on the number of sampled parcels in i. X_i represents the matrix of standardized aggregate and disaggregate architecture and socioeconomic predictors, with β indicating the vector of coefficients for the fixed-effects. Neighborhood-specific random effects are captured by the $Z_i \times b_i$ term; vectors b_i are assumed to follow a multivariate normal distribution with variance-covariance matrix D which is symmetric and positive-definite, while Z_i is a matrix that typically contains a subset of the columns of X_i.

Fixed-effects represent 'average' model parameters whereas random-effects denote neighborhood-specific deviations from 'average' dynamics. We report estimated coefficients on standardized variables. These coefficients represent the effect (on LST) of a standard deviation change for a predictor, keeping the other predictors fixed, and allow us to evaluate the relative significance of the explanatory variables. The random effects b_i and the within-neighborhood errors ε_i are assumed to be independent for different neighborhoods. The neighborhood-specific covariance matrix of the error terms Σ_i is specified to account for spatially correlated parcels within each neighborhood. Specifically, spatial correlation is parameterized by

$$\boldsymbol{cor}\left(\boldsymbol{\varepsilon_i}, \boldsymbol{\varepsilon_j}\right) = \begin{cases} 1 & \textbf{if } \boldsymbol{i} = \boldsymbol{j} \\ \boldsymbol{h}\left(\boldsymbol{\varepsilon_i}, \boldsymbol{\varepsilon_j}, \boldsymbol{c}_0, \boldsymbol{\rho}\right) & \textbf{else} \end{cases} \quad (2)$$

with parameters c_0, ρ denoting the nugget and the range, respectively. Three alternative forms were evaluated for h: Exponential, Gaussian and Spherical (for details on models for spatially correlated residuals see Pinheiro & Bates, 2009; Chapter 5).

Different models were developed for daytime and nighttime temperatures, based on weighted restricted maximum likelihood estimation (REML) that accounted for total lot size. Two model building procedures were implemented. First, the entire set of predictors and interactions of socio-economic and locational factors with architecture metrics was used as input in a regression model. A penalized estimation method with near oracle asymptotic properties, namely adaptive LASSO (Zou, 2006), was used to reduce the initial set (>30) of explanatory variables. Adaptive Lasso performs simultaneous predictor selection and coefficient estimation; it was applied here since stepwise LME building is computationally infeasible when the set of explanatory variables is large. A Box-Cox procedure was applied to identify functional transformations of LST (e.g., logarithmic) that 'linearize' statistical associations; the results of 5-fold cross-validation indicated negligible improvement in predictive performance, hence it was decided to analyze LST in its original scale.

In addition to the explanatory variables presented above, information on date, time and geographical coordinates was used in developing LMEs. Given the predictors identified from adaptive LASSO, mixed effects models were developed following the protocol described in Zuur, Ieno, Walker, Savaliev, and Smith (2009) and the diagnostics presented in Pinheiro and Bates (2009). Specifically, a stepwise implementation of REML was performed to identify significant random effects: predictors with varying effects across

neighborhoods. Another stepwise procedure based on conditional F-tests was implemented to derive the structure of the fixed-effects part, $X_i \times \beta$. Finally, the three alternative spatial correlation structures for the residuals were evaluated against the null model, which assumes independent residuals using Akaike's Information Criterion. The models derived based on the abovementioned procedure are referred to as Model 1_D and Model 1_N, for daytime and nighttime respectively.

The second model building procedure differed from the first in the initial step: instead of adaptive LASSO, a classic stepwise method, namely best subset regression (Kutner, Nachtsheim, & Neter, 2004; James, Witten, Hastie, & Tibshirani, 2013) was implemented using the original set of predictors. Interaction terms were not included since this iterative method is extremely demanding in terms of computation time when the number of predictors is large (>40). The corresponding models for daytime and nighttime LST are dubbed Model 2_D and Model 2_N, respectively.

Mixed-effects models can be used to predict LST at neighborhoods not included in the original sample, based solely on fixed-effects. Therefore, models derived by the two alternative approaches were compared by leave-one-neighborhood-out cross-validation, based on weighted accuracy metrics. Prediction errors within neighborhoods were weighted for parcel size and overall performance was based on weighted averages that accounted for the number of parcels per neighborhood. Three metrics are reported: (1) weighted mean error (WME), a measure of bias; (2) weighted mean absolute error (WMAE); and (3) weighted mean absolute percentage error (WMAPE). To emphasize the significance of predictors related to spatial configuration, the model building procedures were repeated excluding those predictors. The generalization capabilities of these reduced LMEs were compared to the full models using leave-one-neighborhood-out cross-validation.

3. Results

Beyond the descriptive statistics, attention is given to those explanatory variables with strong significance ($p < 0.01$) and higher standardized coefficients.

3.1. Descriptive statistics

Fig. 4 and Table 2 provide the descriptive statistics of the SFR parcels examined. Their mean daytime and nighttime LSTs are 49.6 °C and 23.7 °C, respectively. The range among the parcels was 37.60 °C to 62.41 °C (s.d. = 3.8 °C) for the daytime and 19.11 °C to 30.43 °C (s.d. = 1.4 °C) for the nighttime. Recall that these are land surface, not air, temperatures. Such extreme highs and parcel to parcel variations have been recorded in other studies of Phoenix (Jenerette et al., 2016; Middel, Brazel, Kaplan, & Myint, 2012).

On average, building (SFR structure) occupies 32% of the parcels, with the remainder composed of the other land covers (Table 2). Of those other covers, the PLAND of soil has greatest variation (s.d. = 13.76), reflecting mesic to xeric landscaped parcels, whereas the PLAND for grass had the smallest variation (s.d. = 8.09). The average values for aggregated architecture (parcel level) metrics are 3.57 (LSI), 25,649 (PD), 1.23 (FRAC), and 46.26 (CONTAG), respectively, whereas different ranges of variation existed for individual land-cover types (see Table 2 for metric meanings). As noted above, statistical models were based on standardized predictors; hence the corresponding coefficients can be interpreted despite the different ranges of variation of the original variables.

3.2. Mixed-effects models

Land composition and configuration are both significant in regard to their effects on LST (Tables 3–5). The LMEs that performed best in a leave-one-neighborhood-out cross-validation, included predictors related to both variable types that comprise land architecture. Furthermore, the LMEs derived by ignoring predictors based on configuration, displayed inferior generalization capability (Table 3, parenthetical values). The best performing model for nighttime LST was derived from the best subset regression (Model 2_N) and achieved an accuracy close to 1 °C in terms of WMAE (Fig. 5), a satisfactory result. Daytime temperatures display more variability, influencing the performance of the LMEs with a WMAE slightly below 3 °C (Fig. 5). Accounting for spatially correlated residuals resulted in improved specifications for nighttime, but not for daytime, temperatures. The models also account for temporal increases and decreases LST by the timing of the remote sensing data. The day and night signs of the effects were in accordance with prior expectations, with positive effects on LST as daytime progresses from 11 a.m. to 2 p.m. (Table 5) and negative effects as nighttime advances from about 1:30 a.m. to 4 a.m. (Table 4).

3.2.1. Effects of land composition

The percentage of grass and the presence of a pool proved to be especially significant for nighttime LST, with negative and positive effects on LST, respectively (Model 2_N, Table 4). The effects of grass vary significantly across neighborhoods; this variability could not be explained by land configuration, socio-economic, or locational factors. In addition to these predictors, the suboptimal (in terms of generalization capability relative to the model based on best subsets regression) LME based on adaptive LASSO (Table 3) included the composition of built land and the ratio of living area relative to the total area of the parcel.

The percentage of grass-covered surface in a parcel and the presence of a pool, display negative associations with daytime LST as expected, with high standardized coefficients (Model 1_D and Model 2_D, Table 5). These coefficients reveal a stronger cooling effect of PLAND of trees on daytime temperatures relative to the effect of grass and pool. Again, the daytime effects of grass displayed significant variability across neighborhoods; this variability could not be explained by land configuration, socioeconomic, or geographic factors.

3.2.2. Effects of land configuration

Controlling for the effects of land composition, socio-economic, and locational factors, the LSI for grass is significant for nighttime LST (Model 2_N, Table 4), with a positive standardized coefficient. Larger values of LSI_GRASS (i.e., less compact shape) are associated with higher temperatures; the estimated effect is substantially weaker relative to the significant composition variables. The less parsimonious (and less effective in terms of predictive power) LME for nighttime LST (Model 1_N, Table 4) includes additional class-specific metrics. Interestingly, increasing the edge density (i.e., numerous small patches) of grass is positively associated with nighttime LST. For the aggregated architecture configuration metrics (Model 1_N), the diversity of patches within each parcel (SHDI) holds a positive relationship with LST.

Only aggregated configuration metrics, namely PD and LSI, appear in the set of significant predictors for daytime LST, with standardized coefficients about 50% reduced compared to the effects of PLAND of grass. PD is positively related to LST, whereas the LSI is negatively associated. Based on the estimated coefficients, an increase on the levels of PD and LSI equal to the observed standard deviation of PD and LSI is expected to lead to an increase and decrease, respectively, in daytime LST of about 0.28 °C. PD is not strongly correlated with LSI (Spearman's correlation coefficient is <0.5), hence their effects do not 'cancel out'. The effects of both metrics varied significantly across neighborhoods; this variability could not be explained by socio-economic and locational factors.

3.2.3. Effects of neighborhood socio-economic characteristics

None of the socio-economic predictors, not even the geographical coordinates, were included in the final steps of the model building procedures for LMEs. It was expected that such explanatory variables would account for some of the variability of the random effects that relate with land architecture predictors, as indicated in research using coarser resolution LST data (e.g., Li et al., 2016) and based on recent work elsewhere (Huang & Cadennaso, 2016). On the contrary, it appears that given information on land composition and configuration, the additional variables provide redundant information.

4. Discussion

The two factors of land architecture—composition and configuration of land cover—taken together provide the best modeling results. Considered individually, composition proves to be the most important for the LST of SFR parcels. This result is consistent with those from larger grain assessments of the Phoenix metro area and elsewhere, as well as with a recent fine-grain assessment for Phoenix (Jenerette et al., 2016). It differs, however, from a fine-grain Phoenix study, employing a Normal Moment of Inertia measure of configuration, that found configuration to be more important than composition in affecting LST (Li et al., 2016).

Nighttime LST decreases as the percent of grass cover increases, apparently due to evapotranspiration (Weng, Lu, & Schubring, 2004, Li et al., 2012). Congruent with the findings of Connors et al. (2013), the strength of this relationship varies significantly across neighborhoods (Table 4), perhaps affected by different levels and timing of irrigation by parcel and neighborhood. Pool water absorbs and stores energy as do trees in and under their canopies, releasing it during the evening with positive links to nighttime LST (Myint et al., 2013). Our models for nighttime LSTs identified a strong positive effect related to the presence of pools; on the other hand, the positive effect of trees/shrubs on LST could not be identified, despite occupying about 16% of the parcel areas examined.

A large percentage of building coverage is expected to increase nighttime LST due to reradiated energy built-up during the day and, perhaps, to feedbacks from near surface air warming from the waste heat from air conditioning and refrigeration systems (Salamanca, Georgescu, Mahalov, Moustaoui, & Wang, 2014; Zhou et al., 2011). Given information on grass and pools, the percentage of building, trees/shrubs, and soil cover did not add significant predictive power to our models for nighttime LST. Consistent with previous analyses of LSTs in Phoenix (Connors et al., 2013; Zheng et al., 2014), this result is not surprising since the percentage of grass is negatively correlated with the percentage of buildings (Spearman correlation coefficients equals −0.29).

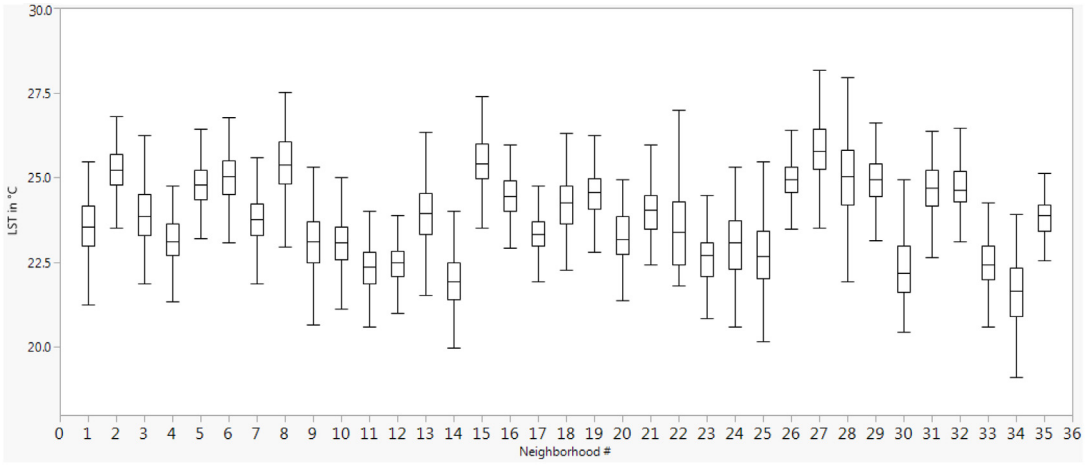

(a) Box plots of average nighttime LST by neighborhood

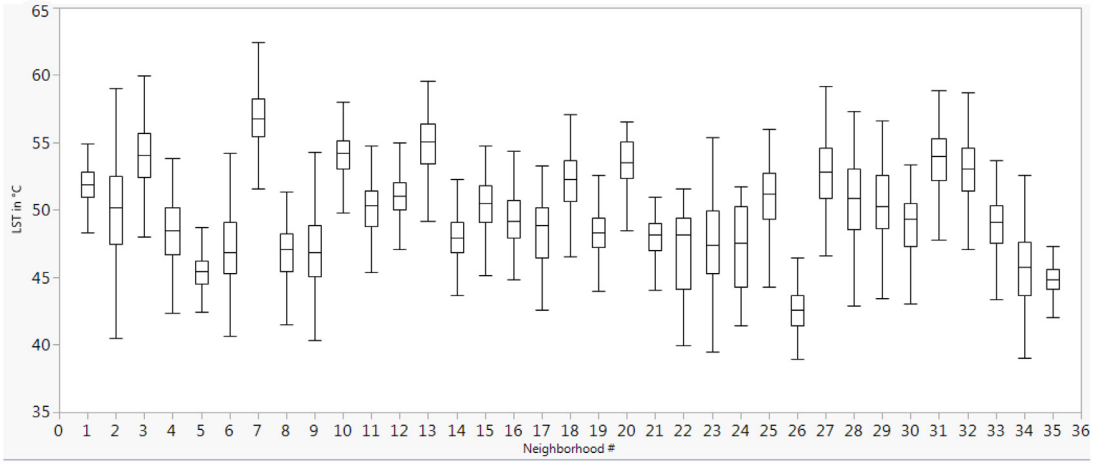

(b) Box plots of average daytime LST by neighborhood

Fig. 4. Distributions of daytime and nighttime land surface temperature (LST) by neighborhood and parcels.

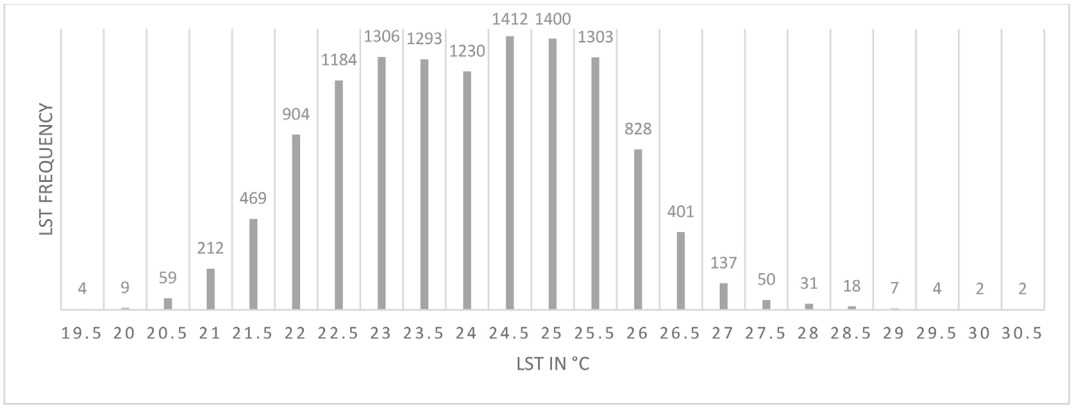

(c) Nighttime LST distribution at parcel level

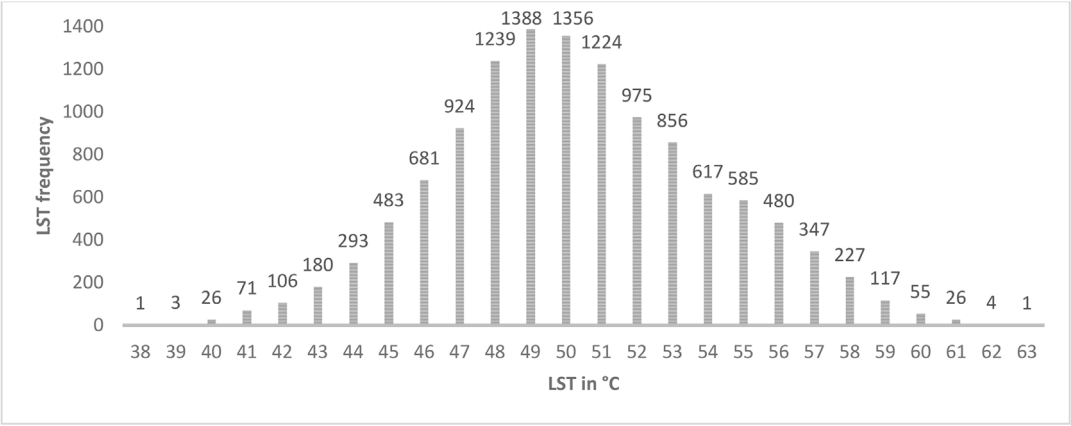

(d) Daytime LST distribution at parcel level

Fig. 4. (*Continued*)

Table 2
Statistical summary of explanatory and predictor variables.

	Variables	Mean	Std Dev	Lower 95% Mean	Std Err Mean	Upper 95% Mean
Aggregated Architecture Metrics	PD	30078.12	11254.32	29882.33	99.89	30273.92
	ED	3290.29	880.40	3274.98	7.81	3305.61
	LSI	3.58	0.80	3.56	0.01	3.59
	FRAC	1.23	0.05	1.23	0.00	1.23
	CONTAG	44.59	9.30	44.43	0.08	44.75
	SHDI	1.22	0.18	1.22	0.00	1.22
Class specific Metrics	PLAND_BUILDING	31.58	11.29	31.38	0.10	31.77
	PD_BUILDING	2171.28	1463.83	2145.81	12.99	2196.74
	ED_BUILDING	1035.92	318.19	1030.38	2.82	1041.45
	LSI_BUILDING	1.48	0.39	1.47	0.00	1.49
	FRAC_BUILDING	1.13	0.09	1.13	0.00	1.14
	PLAND_SOIL	40.28	13.76	40.04	0.12	40.52
	PD_ SOIL	7781.37	5416.51	7687.14	48.07	7875.60
	ED_ SOIL	2530.83	709.21	2518.49	6.29	2543.16
	LSI_ SOIL	3.96	0.98	3.95	0.01	3.98
	FRAC_ SOIL	1.26	0.09	1.26	0.00	1.27
	PLAND_TREE/SHURB	15.91	11.05	15.72	0.10	16.10
	PDTREE/SHURB	9355.13	5445.73	9260.39	48.33	9449.87
	EDTREE/SHURB	1706.08	940.56	1689.72	8.35	1722.44
	LSITREE/SHURB	3.64	1.23	3.62	0.01	3.67
	FRACTREE/SHURB	1.24	0.09	1.24	0.00	1.25
	GRASS	8.88	8.09	8.74	0.07	9.02
	PDGRASS	8206.45	4116.30	8134.84	36.53	8278.06
	EDGRASS	1022.57	586.39	1012.37	5.20	1032.77
	LSIGRASS	3.05	1.10	3.03	0.01	3.07
	FRACGRASS	1.21	0.11	1.21	0.00	1.21
Land Surface Temperature (°C)	Parcel daytime	49.66	3.81	49.59	0.03	49.73
	Parcel nighttime	23.76	1.48	23.74	0.01	23.79

Table 3
Akaike (AIC) and Bayesian (BIC) information criteria, and weighted cross-validation performance criteria for the daytime- and nighttime-specific linear mixed effect models. Weighted cross-validation performance criteria in parentheses correspond to values obtained when model building was applied without predictors related to land configuration (not reported for Model 2_D which does not include such predictors). *h* is the functional form of the spatial correlation structure for the residuals: n_S,r_S denote the nugget and the range of a spherical variogram, n_e,r_e represent the nugget and the range of an exponential variogram, respectively. Generalization performance of alternative models is evaluated using leave-one neighborhood-out cross-validation. Three metrics are reported: Weighted Mean Error (WME), Weighted Mean Absolute Error (WMAE) and Weighted Mean Absolute Percentage Error (WMAPE).

h	Model 1_N		Model 2_N	Model 1_D	Model 2_D
	$n_S = 0.68$, $r_S = 789$	$n_e = 0.61$, $r_e = 813$			
AIC	27714	28556		58594	59723
BIC	27885	28667		58690	59797
WME	0.06 (−0.12)	−0.06 (0.02)		0.16 (0.4)	0.14
WMAE	1.32 (1.80)	1.06 (1.35)		2.73 (3.43)	3.16
WMAPE	0.06 (0.08)	0.05 (0.06)		0.05 (0.07)	0.07

Table 4
Estimated mixed-effects models for nighttime land surface temperature. Fixed effects coefficients are significant with $p < 0.01$. Standard deviations of significant random effects are shown in parentheses, next to the corresponding fixed-effects. Model 1 and 2 correspond to alternative model building procedures.

Variable	Model 1_N		Model 2_N	
	Coefficient	Std Error	Coefficient	Std Error
INTERCEPT	23.89 (1.04)	0.18	23.64 (0.91)	0.30
PLAND_GRASS	−0.40 (0.11)	0.03	−0.18 (0.10)	0.02
POOL	0.23	0.02	0.30	0.02
P_LIVING	0.06	0.01		
PLAND_BUILDING	−0.18 (0.11)	0.02		
LSI_BUILDING	0.07	0.01		
ED_SOIL	−0.13	0.01		
LSI_TREE/SHURB	0.08	0.01		
PD_GRASS	−0.06	0.01		
ED_GRASS	0.15	0.02		
LSI_GRASS			0.10	0.01
CONTAG	0.04	0.01		
SHDI	0.17 (0.12)	0.02		
DATE	0.16	0.04	0.17	0.04
TIME	−0.19	0.02	−0.22	0.02

Table 5
Estimated mixed-effects models for daytime land surface temperature. Fixed effects coefficients are significant with $p < 0.01$. Standard deviations of significant random effects are shown in parentheses, next to the corresponding fixed-effects coefficients. Model 1 and 2 correspond to alternative model building procedures.

Variable/Metrics	Model 1_D		Model 2_D	
	Coefficient	Std Error	Coefficient	Std Error
INTERCEPT	49.37 (2.39)	0.38	49.39 (2.57)	0.44
PLAND_TREE/SHRUB	−0.80	0.04		
PLAND_GRASS	−0.67 (0.17)	0.05	−0.68	0.03
P_LIVING	−0.42	0.03	−0.42	0.03
POOL	−0.68	0.06	−0.61	0.06
PD	0.28 (0.34)	0.08		
LSI	−0.28 (0.44)	0.09		
DATE	0.92	0.13	0.90	0.13
TIME	1.67	0.07	1.73	0.07

Increasing percentages of building and soil cover are expected to increase LST during the day owing to rapid re-radiation, while grass and tree cover lower LST due to evapotranspiration (Zhou et al., 2011). Our statistical models identified the negative effects of grass and tree/shrub cover. Standardized coefficients suggest that increasing the percentage of trees is more effective than grass in lowering LSTs in daytime, consistent with the findings by Myint et al. (2013) and Jenerette et al. (2016). Contrary to expectations, however, holding all other variables constant, the percentage of living area (P_LIVING) was negatively associated with daytime LSTs in our model. P_LIVING is positively associated (Pearson's correlation metric equals 0.2) with the percentage of the parcel covered by a pool, for which our models did not control. Thus the lurking effect of pool size offers a plausible explanation for the significance of P_LIVING.

Land configuration is significant but proves less important than composition, for both daytime and nighttime LST (Tables 4 and 5). This result is based on standardized coefficients and more importantly, on cross-validation experiments where models that did not include each variable type were evaluated in terms of their predictive performance. Grass cover decreases nighttime LST more effectively, however, when patches are clustered; the same association has been reported in analyses of daytime LSTs in Phoenix (Myint et al., 2013). The magnitude of the influences of spatial pattern on daytime LST varied significantly across neighborhoods, consistent with the results in Zheng et al. (2014). The degree of patchiness of all cover types affects daytime LST, either positively or negatively, depending on the land cover. This result complements findings for early nighttime LSTs in Phoenix (Connors et al., 2013). Interestingly, shape complexity plays an important role as well. Increasing PD maintains warmer daytime LSTs, whereas increases in LSI relate to cooler results, as do pools.

It was expected that high income parcels, those near their city cores, and communities with older median age of population would

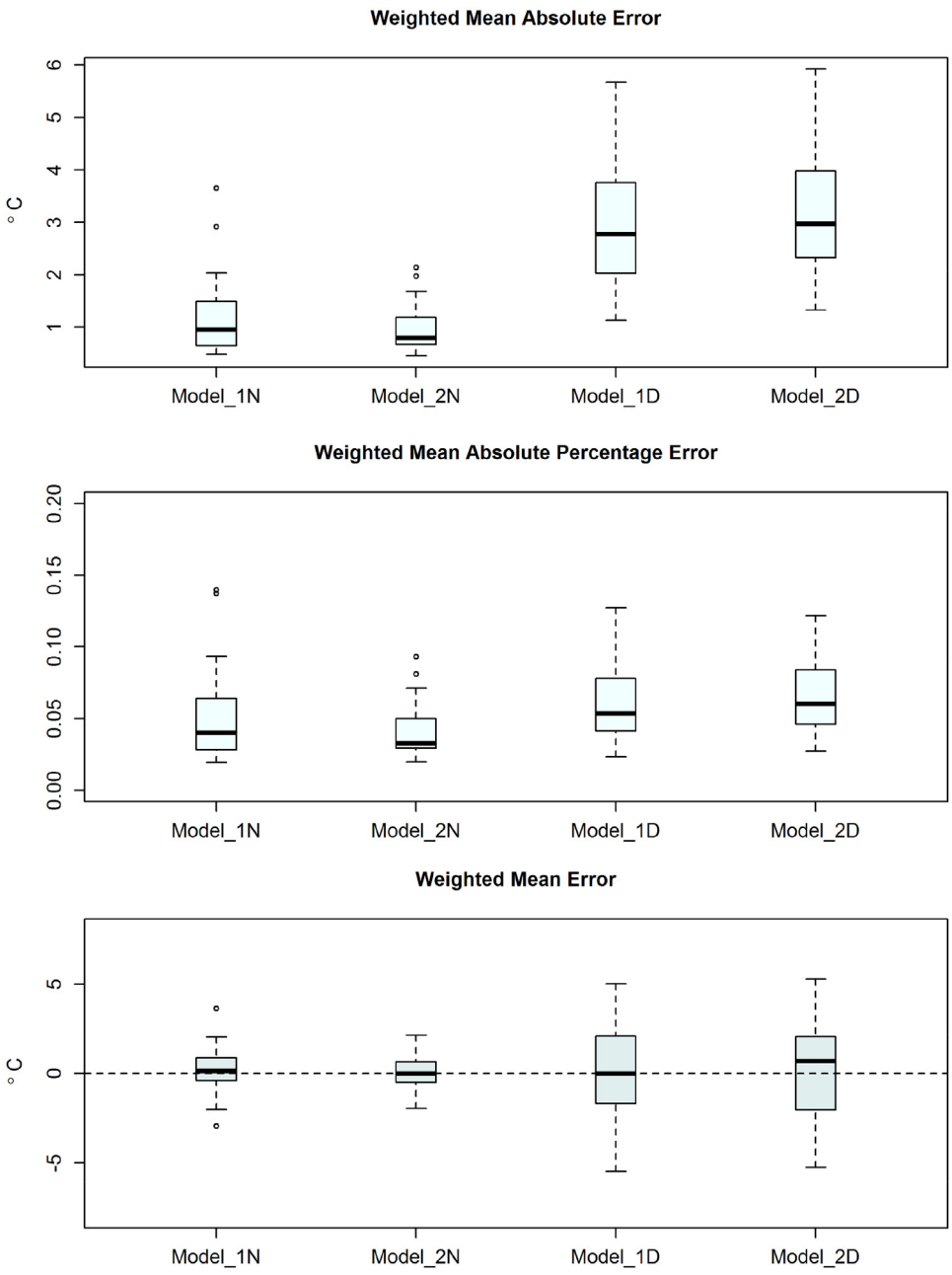

Fig. 5. Distributions of weighted (based on parcel size) mean absolute error (WMAE, top), weighted mean absolute percentage error (WMAPE, middle) and weighted mean error (WME, bottom) across neighborhoods, for daytime- and nighttime-specific linear mixed effects models.

have cooler LST, both day and night. These expectations followed from the association of more vegetation cover, especially grass and tress/shrubs, with older, more expensive neighborhoods based "desert oasis" or mesic landscaping, and more swimming pools, on average, linked to the capacity to afford them. In contrast, low income parcels and parcels near their city fringe were expected to have a positive impact on nighttime and daytime LST. The former result follows from the documented decrease in vegetation cover among low-income parcels (Declet-Barreto, Brazel, Martin, Chow, & Harlan, 2013; Harlan, Brazel, et al., 2006) and the latter, perhaps, due the prevalence of "xeric-scape" parcels among the newer residential developments on the outer edges of the metroplex. Such explanatory variables were significant only at the first stage of our analyses, which did not account for nested, neighborhood-specific data structures and spatially correlated parcels within the same neighborhood. Our statistical models suggest that at the parcel level, given information on land composition and configuration, socioeconomic variables are not significant in explaining the variability of daytime or nighttime LST. This finding does not contradict other work indicating that lower income areas tend to correspond to higher LST or UHI hotspots, such as those generated by the high proportion of impervious surfaces in low income areas of Baltimore, MD (Huang, Zhou, & Cadenasso, 2011) or the low proportion of vegetation cover common to Hispanic neighborhoods in Phoenix (e.g., Harlan, Budruk, Gustafson, Larson, & Ruddell, 2006). Rather, landscaping is a more a proximate factor influencing LST than are socioeconomic variables (Li et al., 2016), and our level of detail concerning land-cover mutes the predictive performance of socioeconomic variables. Indeed, a recent article that focused on the Baltimore area (census block level) found that land cover had a stronger association with LST than other classes of variables,

but that social variables apparently affect land cover, and thus LST (Huang & Cadenasso, 2016).

Our best performing model for nighttime LST did not identify a significant effect for the percentage of residential building cover (PLAND_BUILDING), given information on the presence of a pool and the percentage and the shape index of grass. The less parsimonious model, however, indicates a negative association between residential building cover and LST. In contrast, Myint et al. (2013) found a positive correlation between them. The different results may reflect the different spatial scales and areas of assessment used to determine LST. Myint et al. (2013) employed 90 m ASTER-derived LST data to address segments of the urban area, not individual parcels. In addition, they combined all water sources (i.e., pools and ponds) and vegetation in a city segment regardless of their presence on individual parcels. In contrast, our study employs 6.8 m MASTER-derived LST data, which can capture roof areas from the remainder of the land covers of parcels, and did not include common water bodies and vegetation, which is not part of analyzed parcels. Our disaggregated model result is consistent with that from Atlanta, GA (USA) in which smaller buildings (e.g., residential units) were found to be beneficial for reducing nighttime temperatures because roofs release thermal energy during this time (Chun & Guhathakurta, 2016).

4.1. Urban management and planning implications

It is increasingly recognized that the relationship between LST and land architecture has important implications for mitigating the SUHI effects (Weng et al., 2004; Hamada and Ohta, 2010; Zhou et al., 2011; Jenerette et al., 2016; Li et al., 2012; Li et al., 2016), with obvious implications for water withdrawals (Wentz et al., 2016), especially in hot, arid environments. Our study suggests that the effectiveness of land cover in this mitigation involves a full array of urban land covers, even at the fine-grain (i.e., parcel) level. While land-cover composition, such as the amount of green space, is the most important factor in this mitigation, it can be enhanced by patch clustering and shape compactness, depending on the land cover. An initial lesson appears to be that compactly shaped and concentrated patches of vegetation, foremost grass, is especially important in decreasing nighttime LST, whereas parcels maintaining larger land-cover units of irregular shape decrease daytime LST. Balancing the spatial distribution of land-cover types and optimizing their spatial patterns and shape appears to be a means to reducing LST among SFR parcels, or at least some of its consequences, and if replicated sufficiently, at the neighborhood level and beyond.

An open question is the consistency of the configuration outcomes across different spatial scales. Are residential level outcomes the same for ascending units of urban space? This question demands more attention as does the optimal design of land covers in regard to the tradeoffs between daytime and nighttime LST. In addition, land architecture has large impacts on water use and runoff, aquifer recharge, biological corridors, and urban aesthetics, among other environmental services, and urban sustainability involves tradeoffs among these and other services, not just attention to the UHI effect. In the Phoenix case, the strong mitigation role of grass holds tradeoffs with large water requirements in a water-sparse environment. Regardless, research on the relationship between land architecture and LST indicates that land-cover configuration plays an important role in the functioning of these services, and the search for design principles for new residences and reconfiguration of older parcels to mitigate extreme heat or other disservices warrant attention. Ultimately, of course, these considerations need to address above ground temperature.

4.2. Limitations

This research has enlarged the number and diversity of neighborhoods and parcels examined compared to other studies, and our assessment included both daytime and nighttime LST. Yet, a more complete aerial coverage and a larger number of days on which fine-grain LSTs could be generated may provide more revealing results. While the method employed to determine emissivity and, hence, "corrected" LST is common to studies of this kind, anisotropy errors may be created by the 3D characteristics of the land architecture not considered here, such as varying canopy levels and housing density by neighborhoods (Krayenhoff & Voogt 2016). Despite the fine-grain of our LST (6.8 m) and land-cover data (1 m), the spatial matching involves modest aggregation and averaging of LST per pixel. As well, access to parcel specific socio-economic data may have altered our results. Finally, we only examined the relationship of LST and land architecture for SFR parcels. Other parcel types, such as multiple family residential, commercial, and recreational parcels or their bundling were not addressed. Future research will extend study sites beyond SFR.

5. Concluding remarks

Understanding the relationship between land architecture and SUHI effects is important for mitigating extreme heat and its consequences, especially in desert cities but increasingly for cities residing in the tropics to mid-latitudes where global warming is expected to increase extreme heat events. Our research, using fine resolution, parcel level data and linear mixed effects models, corroborates emerging research findings elsewhere that both the composition and configuration of land systems affects LST, contributing to SUHI. It elaborates those findings, however, by demonstrating that (1) controlling for land composition, land configuration at the parcel level proves to be a significant factor affecting LST, and (2) socioeconomic neighborhood characteristics are not significant in explaining daytime and nighttime LSTs for SFRs, given information on land composition and configuration. Such controls also indicate that the interplay among explanatory variables results in their different directional influences on LST at different times of day, as well as by different land architecture metrics. These results point to characteristics of individual land covers and their parcel aggregates that ameliorate LST, foremost during the night. Taken together, they indicate the need for more research on the fine-grain land architecture of the "city-scape", its impacts of the SUHI, and its possible use to reshape individual parcels, neighborhoods, and urban areas to achieve a more temperature friendly outcome for desert cities.

Acknowledgements

This research was supported by the National Science Foundation (NSF) under Grant No. SES-0951366, NSF DNS Grant No. 1419593 and USDA NIFA Grant No. 2015-67003-23508, and by the Central Arizona-Phoenix Long-Term Ecological Research project (NSF BCS-1026865). The research was undertaken in the Environmental Remote Sensing and Geoinformatics Lab with additional support from the Gilbert F. White Fellowship, Arizona State University.

References

Bernstein, L. S., Adler-Golden, S. M., Sundberg, R. L., Levine, R. Y., Perkins, T. C., Berk, A., et al. (2005). Validation of the quick atmospheric correction (QUAC) algorithm for VNIR-SWIR multi- and hyperspectral imagery. *SPIE proceedings, algorithms and technologies for multispectral, hyperspectral, and ultraspectral imagery proceedings of SPIE, 5806*, 668–678.

Brown, R. D., & Corry, R. C. (2011). Evidence-based landscape architecture: The maturing profession. *Landscape and Urban Planning, 100*, 327–329.

Buyantuyev, A., & Wu, J. (2009). Urbanization alters spatiotemporal patterns of ecosystem primary production: A case of the Phoenix metropolitan area, USA. *Journal of Arid Environments*, *73*.
Chang, Y., Han, C., Fan, K., Chen, S. K., & Chang, J. (2002). A modular eigen subspace scheme for high-dimensional data classification with NASA MODIS/ASTER (MASTER) airborne simulator data sets of Pacrim II project. *Imaging spectrometry VIII proceedings of SPIE*, *4816*, 426–436.
Chow, W. T. L., Chuang, W., & Gober, P. (2012). Vulnerability to extreme heat in metropolitan phoenix: Spatial, temporal, and demographic dimensions. *The Professional Geographer*, *64*, 286–302.
Chun, B., & Guhathakurta, S. (2016). The impacts of three-dimensional surface characteristics on urban heat islands over the diurnal cycle. *Professional Geographer*, http://dx.doi.org/10.1080/00330124.2016.1208102
City of Phoenix. (2010). *Tree and shade master plan*. http://www.phoenix.gov/parkssite/Documents/0719557.pdf
Clark, W. C. (2007). Sustainability science: A room of its own. *Proceedings of the National Academy of Sciences*, *104*, 1737–1738.
Connors, J. P., Galletti, C. S., & Chow, W. T. (2013). Landscape configuration and urban heat island effects: Assessing the relationship between landscape characteristics and land surface temperature in Phoenix, Arizona. *Landscape Ecology*, *28*, 271–283.
Coseo, P., & Larsen, L. (2014). How factors of land use/land cover, building configuration, and adjacent heat sources and sinks explain Urban Heat Islands in Chicago. *Landscape and Urban Planning*, *125*, 117–129.
Cox, K. R. (1969). The voting decision in a spatial context. *Progress in Geography*, *1*, 81–117.
Declet-Barreto, J., Brazel, A. J., Martin, C. A., Chow, W. T., & Harlan, W. T. (2013). Creating the park cool island in an inner-city neighborhood: Heat mitigation strategy for Phoenix, AZ. *Urban Ecosystems*, *16*, 617–635.
Donovan, G. H., & Butry, D. T. (2009). The value of shade: Estimating the effect of urban trees on summertime electricity use. *Energy and Buildings*, *41*, 662–686.
Erell, E., Pearlmutter, D., & Williamson, T. (2012). *Urban microclimate: Designing the spaces between buildings*. New York: Routledge.
Fan, C., Myint, S. W., & Zheng, B. (2015). Measuring the spatial arrangement of urban vegetation and its impacts on seasonal surface temperatures. *Progress in Physical Geography*, *39*, 119–121.
Fast, J. D., Torcolini, J. C., & Redman, R. (2005). Pseudo vertical temperature profiles and the urban heat island measured by a temperature datalogger network in Phoenix, Arizona. *Journal of Applied Meteorology*, *44*, 3–13.
Finch, W. H., Bolin, J. E., & Kelley, K. (2014). *Multilevel modeling using R*. Boca Raton, FL: CRC Press.
Forman, R. T. T. (1990). Ecologically sustainable landscapes: the role of spatial configuration. In I. S. Zonnelfeld, & R. T. T. Forman (Eds.), *Changing landscapes: An ecological perspective* (pp. 261–278). New York: Springer.
Forman, R. T. T. (2014). *Urban ecology: Science of cities*. Cambridge: Cambridge Cniversity Press.
Gago, E. J., Roldán, J., Pacheco-Torres, R., & Ordoñez, J. (2013). The city and urban heat islands: A review of strategies to mitigate adverse effects. *Renewable and Sustainable Energy Reviews*, *25*, 749–758.
Giridharan, R., Lau, S. S. Y., Ganesan, S., & Givoni, B. (2007). Urban design factors influencing heat island intensity in high-rise high-density environments of Hong Kong. *Building and Environment*, *42*, 3669–3684.
Grossman-Clarke, S., Zehnder, J. A., Loridan, T., & Grimmond, C. S. B. (2010). Contribution of land use changes to near-surface air temperatures during recent summer extreme heat events in the Phoenix metropolitan area. *Journal of Applied Meteorology and Climatology*, *49*, 1649–1664.
Grossman-Clarke, S., Schubert, S., Clarke, T. A., & Harlan, S. L. (2014). Extreme summer heat in Phoenix, Arizona (USA) under global climate change (2041–2070). *Die Erde–Journal of the Geographical Society of Berlin*, *145*, 49–61.
Hamada, S., & Ohta, T. (2010). Seasonal variations in the cooling effect of urban green areas on the surrounding urban areas. *Urban Forestry and Urban Greening*, *9*, 15–24.
Harlan, S. L., Brazel, A. J., Prashad, L., Stefanov, W. L., & Larsen, L. (2006). Neighborhood microclimates and vulnerability to heat stress. *Social Science & Medicine*, *63*, 2847–2863.
Harlan, S. L., Budruk, M., Gustafson, A., Larson, K., Ruddell, D., et al. (2006). *Highlights phoenix area social survey: Community and environment in a desert city*. Tempe, AZ: Global Institute of Sustainability, Arizona State University. Contribution no. 4. CAP-LTER.
Hart, M. A., & Sailor, D. J. (2009). Quantifying the influence of land-use and surface characteristics on spatial variability in the urban heat island. *Theoretical and Applied Climatology*, *95*, 397–406.
Hawkins, T. W., Brazel, A. J., Stefanov, W. L., Bigler, W., & Saffell, E. M. (2004). The role of rural variability in urban heat island determination for Phoenix, Arizona. *Journal of Applied Meteorology*, *43*, 476–486.
Hook, J. S., Myers, J. J., Thome, J. K., Fitzgerald, M., & Kahle, B. A. (2001). The MODIS/ASTER airborne simulator (MASTER) – A new instrument for earth science studies. *Remote Sensing of Environment*, *76*, 93–102.
Huang, G., & Cadenasso, M. L. (2016). People, landscape and urban heat islands: Dynamics among neighborhood social conditions, land cover, and surface temperatures. *Landscape Ecology*, *31*, 2507-25-15.
Huang, L., Li, J., Zhao, D., & Zhu, J. (2008). A fieldwork study on the diurnal changes of urban microclimate in four types of ground cover and urban heat island of Nanjing, China. *Building and Environment*, *43*, 7–17.
Huang, G., Zhou, W., & Cadenasso, M. L. (2011). Is everyone hot in the city? Spatial pattern of land surface temperatures, land cover and neighborhood socioeconomic characteristics in Baltimore, MD. *Journal of Environmental Management*, *92*, 1753–1759.
James, G., Witten, D., Hastie, T., & Tibshirani, R. (2013). *An introduction to statistical learning*. Berlin: Springer.
Jenerette, G. D., Harlan, S. L., Stefanov, W., & Martin, C. (2011). Ecosystem services and urban heat riskscape moderation: Water, green spaces, and social inequality in Phoenix, USA. *Ecological Applications*, *21*, 2637–2651.
Jenerette, G. D., Harlan, S. L., Buyantuev, A., Stefanov, W., Declet-Barreto, J., Ruddell, B. L., et al. (2016). Micro-scale urban surface temperatures are related to land-cover features and residential heat related health impacts in Phoenix, AZ, USA. *Landscape Ecology*, *31*, 745–760.
Johnston, R., Propper, C., Sarker, R., Jones, K., Bolster, A., et al. (2005). Neighbourhood socialcapital and neighbourhood effects. *Environment and Planning A*, *37*, 1443–1459.
Keys, E., Wentz, E. A., & Redman, C. L. (2007). The spatial structure of land use from 1970 to 2000 in the Phoenix, Arizona, metropolitan area. *Professional Geographer*, *59*, 131-147.
Kleerekoper, L., van Esch, M., & Baldiri Salcedo, T. (2012). How to make a city climate-proof, addressing the urban heat island effect. *Resources, Conservation and Recycling*, *64*, 30–38.
Krayenhoff, E. S., & Voogt, J. A. (2016). Daytime thermal anisotropy of urban neighborhoods: morphological causation. *Remote Sensing*, *8*, 108.
Kutner, M., Nachtsheim, C., & Neter, J. (2004). *Applied linear regression models* (4th ed.). McGraw-Hill.
Li, J. J., Wang, X. R., Wang, X. J., Ma, W. C., & Zhang, H. (2009). Remote sensing evaluation of urban heat island and its spatial pattern of the Shanghai metropolitan area, China. *Ecological Complexity*, *6*, 413–420.
Li, X., Zhou, W., Ouyang, Z., Xu, W., & Zheng, H. (2012). Spatial pattern of greenspace affects land surface temperature: Evidence from the heavily urbanized Beijing metropolitan area China. *Landscape Ecology*, *27*, 887–898.
Li, X., Li, W., Middel, A., Harlan, S. L., Brazel, A., & Turner, B. L., II. (2016). Remote sensing of the surface urban heat island and land architecture in Phoenix, Arizona: Combined effects of land composition and configuration and cadastral-demographic-economic factors. *Remote Sensing of Environment*, *174*, 233–243.
Li, D., Bou-Zeid, E., & Oppenheimer, M. (2014). The effectiveness of cool and green roofs as urban heat island mitigation strategies. *Environmental Research Letters*, *9*, 055002.
Li, X., Myint, S. W., Zhang, Y., Galletti, C., Zhang, X., & Turner, B. L., II. (2014). Object-based land-cover classification for metropolitan phoenix, Arizona, using aerial photography. *International Journal of Applied Earth Observations and GeoinSformation*, *33*, 321–330.
McCarthy, M. P., Best, M. J., & Betts, R. A. (2010). Climate change in cities due to global warming and urban effects. *Geophysical Research Letters*, *37*, 9.
McGarigal, K., & Marks, B. J. (1995). *FRAGSTATS: Spatial pattern analysis program for quantifying landscape structure*. Portland (OR): USDA Forest Service, Pacific Northwest Research Station. General Technical Report PNW-GTR-351.
McGarigal, K., Cushman, S. A., & Ene, E. (2012). *FRAGSTATS v4: Spatial pattern analysis program for categorical and continuous maps*. Amherst, MA: University of Massachusettes. URL http://www.umass.edu/landeco/research/fragstats/fragstats.html
Middel, A., Brazel, A. J., Kaplan, S., & Myint, S. W. (2012). Daytime cooling efficiency and diurnal energy balance in Phoenix, Arizona, USA. *Climate Research*, *54*, 21–24.
Middel, A., Häb, K., Brazel, A., Martin, C., & Guhathakurta, S. (2014). The impact of urban form and design on mid-afternoon microclimate in Phoenix local climate zones. *Landscape and Urban Planning*, *122*, 16–28.
Mitchell, M. G. E., Bennett, E. M., & Gonzalez, A. (2013). Linking landscape connectivity and ecosystem service provision: Current knowledge and research gaps. *Ecosystems*, *16*, 894–908.
Myint, S. W., Wentz, E. A., Brazel, A. J., & Qualttrochi, D. A. (2013). The impact of distinctive anthropogenic and vegetation features on urban warming. *Landscape Ecology*, *28*, 959–978.
Myint, S. W., Zheng, B., Talen, E., Fan, C., Kaplan, S., Middel, A., et al. (2015). Does the spatial arrangement of urban landscape matter? Examples of urban warming and cooling in Phoenix and Las Vegas. *Ecosystem Health and Sustainability*, *1*, 1–15.
Myint, S. W. (2012). Effects of the spatial pattern of vegetation cover on urban warming in a desert city. In X. Yang, & J. Li (Eds.), *Advances in mapping from aerospace imagery: Techniques and applications* (pp. 261–278). Boca Raton, FL: CRC Press.
Oke, T. R. (1981). Canyon geometry and the nocturnal urban heat island: Comparison of scale model and field observations. *Journal of Climatology*, *1*, 237–254.
Pinheiro, J. C., & Bates, D. M. (2009). *Mixed effects models in S and S-plus*. Berlin: Springer.
Saha, M. V., Davis, R. E., & Hondula, D. M. (2014). Mortality displacement as a function of heat event strength in 7 US cities. *American Journal of Epidemiology*, *179*, 467–474.
Salamanca, F., Georgescu, M., Mahalov, A., Moustaoui, M., & Wang, M. (2014). Anthropogenic heating of the urban environment due to air conditioning. *Journal of Geophysical Research*, *119*, 5949–5965.
Santamouris, M. (2013). Using cool pavements as a mitigation strategy to fight urban heat island—A review of the actual developments. *Renewable and Sustainable Energy Reviews*, *26*, 224–240.

Seto, K., & Reenberg, A. (Eds.). (2014). *Rethinking global land use in an urban era*. Cambridge, MA: MIT Press.
Shashua-Bar, L., Pearlmutter, D., & Erell, E. (2009). The cooling efficiency of urban landscape strategies in a hot dry climate. *Landscape and Urban Planning*, *92*, 179–186.
Shashua-Bar, L., Pearlmutter, D., & Erell, E. (2011). The influence of trees and grass on outdoor thermal comfort in a hot-arid environment. *International Journal of Climatology*, *31*, 1498–1506.
Silva, H. R., Phelan, P. E., & Golden, J. S. (2010). Modeling effects of urban heat island mitigation strategies on heat-related morbidity: A case study for Phoenix, Arizona, USA. *International Journal of Biometeorology*, *54*, 13–22.
Solecki, W. D., Rosenzweig, C., Parshall, L., Pope, G., Clark, M., Cox, J., et al. (2005). Mitigation of the heat island effect in urban New Jersey. *Environmental Hazards*, *6*, 39–49.
Stewart, I. D., & Oke, T. R. (2012). Local climate zones for urban temperature studies. *Bulletin of the American Meteorological Society*, *93*, 1879–1900.
Su, W., Gu, C., & Yang, G. (2010). Assessing the impact of land use/land cover on urban heat island pattern in Nanjing City, China. *Journal of Urban Planning and Development*, *136*, 365–372.
Taha, H. (1997). Urban climates and heat islands: Albedo, evapotranspiration, and anthropogenic heat. *Energy and Buildings*, *25*, 99–103.
Turner, B. L., II, Lambin, E. F., & Reenberg, A. (2007). The emergence of land change science for global environmental change and sustainability. *Proceedings of the National Academy of Sciences*, *104*, 20666–20671.
Turner, B. L., II, Janetos, A. C., Verbug, P. H., & Murray, A. T. (2013). Land system architecture: Using land systems to adapt and mitigate global environmental change. *Global Environmental Change*, *23*, 395–397.
Turner, B. L., II. (2017). Land system architecture for urban sustainability: New directions for land system science illustrated by application to the urban heat island problem. *Journal of Land Use Science*, *12* [forthcoming].
Weng, Q., Lu, D., & Schubring, J. (2004). Estimation of land surface temperature—Vegetation abundance relationship for urban heat island studies. *Remote Sensing of Environment*, *89*, 467–483.
Wentz, E. A., Rode, S., Li, X., Tellman, E. M., & Turner, B. L., II. (2016). Impact of homeowner association (HOA) landscaping guidelines on residential water use. *Water Resources Research*, *52*, 3373–3386.
Wu, J., Jenerette, G. D., Buyantuyev, A., & Redman, C. L. (2011). Quantifying spatiotemporal patterns of urbanization: The case of the two fastest growing metropolitan regions in the United States. *Ecological Complexity*, *8*, 1–8.
Wu, J. (2013). Landscape sustainability science: Ecosystem services and human well-being changing landscapes. *Landscape Ecology*, *28*, 999–1023.
Yu, K. J., Li, D. H., & Ji, Q. P. (2001). Ecological design for landscape and city: Concepts and principles. *Chinese Landscape Architecture*, *6*, 3–10.
Zhang, H., Qi, Z. F., Ye, X. Y., Cai, Y. B., Ma, W. C., & Chen, M. N. (2013). Analysis of land use/land cover change, population shift, and their effects on spatiotemporal patterns of urban heat islands in metropolitan Shanghai, China. *Applied Geography*, *44*, 121–133.
Zheng, B., Myint, S. W., & Fan, C. (2014). Spatial configuration of anthropogenic land cover impacts on urban warming. *Landscape and Urban Planning*, *130*, 104–111.
Zhou, W., Huang, G., & Cadenasso, L. M. (2011). Does spatial configuration matter? Understanding the effects of land cover pattern on land surface temperature in urban landscapes. *Landscape and Urban Planning*, *102*, 54–63.
Zou, H. (2006). The adaptive lasso and its oracle properties. *Journal of the American Statistical Association*, *101*, 1418–1429.
Zuur, A., Ieno, E. N., Walker, N., Savaliev, A. A., & Smith, G. M. (2009). *Mixed effects models and extensions in ecology with R*. Berlin: Springer.